Theory of free-bound transitions in channeling radiation

A. W. Sáenz

Naval Research Laboratory, Washington, D.C. 20375-5000
and Department of Physics, Catholic University of America, Washington, D.C. 20064

A. Nagl and H. Überall

Department of Physics, Catholic University of America, Washington, D.C. 20064
(Received 5 May 1987; revised manuscript received 30 December 1987)

On the basis of a single-string model, we derive formulas for the transition strengths of free-bound transitions of axially channeled electrons. We illustrate the theory by numerical calculations of these strengths for 3.5-MeV electrons in Si. Experimental evidence for such transitions has been obtained previously [J.U. Andersen *et al.*, Nucl. Instrum. Methods **194**, 209 (1982)] and is in good qualitative agreement with our calculations.

I. INTRODUCTION

In the present study, we will consider a type of radiation which conceptually is intermediate between the well-known phenomena of coherent bremsstrahlung and channeling radiation, namely, the radiation given off during transitions of charged leptons from a free to a bound state of transverse motion as a leptons traverse a crystal in one of its channels. We will refer to these as "free-bound (fb) transitions" and shall calculate here the transition strength (or radiation intensity) corresponding to these transitions. No such calculations appear in the literature, while the related radiation effects of coherent bremsstrahlung [corresponding to free-free (ff) transitions] and of channeling radiation [corresponding to bound-bound (bb) transitions] have been the subject of extensive previous investigation.[1]

The physics of the radiation emitted by charged leptons (i.e., electrons or positrons) while traversing a crystal has a long history. Ordinary bremsstrahlung of leptons interacting with an isolated atom of matter[2] gets modified if the atoms are arranged in a crystalline structure, and interference effects appear, as first pointed out by Williams.[3] The ensuing phenomenon of "coherent bremsstrahlung" was studied theoretically by Überall using the Born approximation,[4,5] and the effect was subsequently verified experimentally by Diambrini.[6] Coherent bremsstrahlung furnishes an intense source of quasimonochromatic radiation which is tunable and linearly polarized to a high degree.[7] Sources of this radiation were set up at a number of electron accelerator laboratories and were used to carry out nuclear physics experiments.[8,9]

The regular array of lattice atoms gives rise to geometrical "channels" in a crystal, and charged particles traversing the crystal may become trapped in such a channel, due to the screened Coulomb forces exerted on them by the atoms of the crystal planes ("planar channeling") or axes ("axial channeling").[10] Positively charged particles will be channeled between planes or axes, while negatively charged particles will be trapped along a plane or an axis, carrying out classically an oscillatory motion

around an equilibrium position of their transverse motion in the channel. Kumakhov[11] predicted that this oscillatory motion gives rise to another type of radiation, the so-called "channeling radiation." The existence of this radiation was experimentally confirmed by Berman *et al.*,[12] and it was shown later by Andersen *et al.*[13] that coherent bremsstrahlung and channeling radiation can be considered as but two different aspects of one and the same underlying physical process.

A connection between the two phenomena can be established by describing the motion of leptons in the crystal in a fashion that separates their longitudinal motion relative to a (planar or axial) crystal channel from their transverse motion (the latter being nonrelativistic even at very high energy, provided the total momentum points sufficiently closely along the direction of the channel). While the longitudinal motion of the lepton is essentially free, the transverse motion relative to crystal planes or axes (which, to a good approximation, may be considered as being continuously charged planes or continuously charged "strings," respectively[10]) is then that of a charged particle bound by these planes or axes. Quantum mechanically, the leptons in the potential of the planes or strings possess a series of discrete bound levels followed by a continuum at higher transverse energies. The incident lepton beam populates both the bound and the continuum states in a way that depends sensitively on the angle of incidence, and subsequently radiative transitions of the leptons from higher to lower states take place spontaneously.

The radiation emitted by leptons transitioning from a bound state to a bound state (bb transitions) corresponds to "channeling radiation" proper, as predicted by Kumakhov[11] and observed by Berman *et al.*[12] The radiation from free-free (ff) transitions, i.e., from one continuum state to another, is identical with "coherent bremsstrahlung" as described by Überall[4] (without considering transverse binding effects) and observed by Diambrini *et al.*[6,14] In addition, there will be radiative transitions leading from a continuum state to a bound state (fb); the corresponding radiation has alternately been classified as

channeling radiation (third reference of Ref. 12) or as coherent bremsstrahlung[8] but it actually should be viewed as being in a separate class.

This fb radiation has been observed experimentally.[13] It can be distinguished from bb or ff radiation by the variation of its energy with the angle of incidence of the leptons relative to a crystal plane or axis, which is essentially angle independent for bb transitions, approximately linear for ff transitions, and approximately quadratic for fb transitions.[8,13] The radiation from fb transitions has been recorded experimentally,[13] and on a three-dimensional plot of intensity versus both photon energy and angle of incidence, it appears in the form of characteristic horseshoe-shaped ridges of lower height, located in front of towering bb pinnacles and opening up away from the latter (see, e.g., Fig. 9 of the second reference of Ref. 13, reproduced below). While as mentioned, theories for ff and bb radiation intensities are available, no theory for fb transitions seems to appear in the literature except for one radiation-intensity calculation for planar channeling of 4-MeV electrons in Si (first of Ref. 13). In the following, we shall provide such a theoretical calculation of fb-transition intensity in axial channeling based on a fairly simple model. A preliminary account of this work has been given previously as a conference report.[15]

II. WAVE FUNCTIONS AND INTENSITY FORMULAS

The transition probabilities of radiative fb transitions of axially channeled electrons in crystals will be calculated here on the basis of the following simple model, which should be accurate enough for an exploratory theoretical investigation of the phenomenon. The initial electron wave function is taken to be a free plane wave ψ_f, and the final electron is assumed to be transversely bound in the field of a single continuous string along the axis, with wave function ψ_b. This approach ignores the Bloch-function nature of ψ_b in a periodic crystal, but is results are the same as those which would be obtained by taking ψ_b as the product of a longitudinal plane wave and a transverse Bloch function given by the lowest-order tight-binding approximation. For comparison purposes we will also derive corresponding formulas for bb transitions using the same model.

The initial- and final-electron wave functions are approximated by

$$\psi_f(\mathbf{r}) = \frac{1}{L^{3/2}} \left[\frac{E+m}{2E} \right]^{1/2} \left[\begin{array}{c} u \\ \dfrac{\sigma \cdot \mathbf{p} u}{E+m} \end{array} \right] e^{i\mathbf{p}\cdot\mathbf{r}} \qquad (1a)$$

and

$$\psi_b(\mathbf{r}) = \frac{1}{L^{1/2}} \left[\frac{E'+m}{2E'} \right]^{1/2} \left[\begin{array}{c} u \\ \dfrac{\sigma \cdot \mathbf{p}_0 u}{E'+m} \end{array} \right] \varphi_{nl}(\mathbf{r}_\perp) e^{i p_z' z} , \qquad (1b)$$

respectively. Here L is the length of the string; E, E' are the initial and final-electron energies, and m is the electron mass; $\mathbf{p}$ is the initial electron momentum vector and $\mathbf{p}_0 = (-i\nabla_\perp, p_z')$, the subscript $\perp$ denoting a component transverse to the z axis and p_z' the z component of the

final momentum. Moreover, the transversely bound wave functions $\varphi_{nl}(\mathbf{r}_\perp)$ are of the form

$$\varphi_{nl}(\mathbf{r}_\perp) = (2\pi)^{-1/2} e^{il\phi} R_{nl}(\rho) , \qquad (2a)$$

where $\rho \equiv |\mathbf{r}_\perp|$ and ϕ are polar coordinates in the $\mathbf{r}_\perp$ plane. These wave functions satisfy the Schrödinger equation for transverse motion in the string potential $V(\mathbf{r}_\perp)$:

$$-(1/2E)\nabla_\perp^2 \varphi_{nl}(\mathbf{r}_\perp) + V(\mathbf{r}_\perp)\varphi_{nl}(\mathbf{r}_\perp) = \epsilon_{nl}\varphi_{nl}(\mathbf{r}_\perp) , \qquad (2b)$$

where E and ϵ_{nl} are related by

$$\epsilon_{nl} = \frac{E^2 - m^2 - p_z^2}{2E} \qquad (3a)$$

in the present approximation. This means that the state $\varphi_{nl}(\mathbf{r}_\perp)$ can be populated only if the initial momentum $\mathbf{p}$ is appropriately chosen. We normalize $\varphi_{nl}(\mathbf{r}_\perp)$ as follows:

$$\int |\varphi_{nl}(\mathbf{r}_\perp)|^2 d^2 r_\perp = 1 . \qquad (3b)$$

The differential intensity of radiation emitted in the fb transition is[2]

$$dI_\lambda = 2\pi\delta(E - E' - k)k \, |H_{fb}^{(\lambda)}|^2 \frac{L^3 d^3 k}{(2\pi)^3} \frac{L \, dp_z'}{2\pi} , \qquad (4a)$$

where $\lambda = 1,2$ labels the photon polarization direction, $k = |\mathbf{k}|$ is the photon energy, and the absolute value squared of the pertinent matrix element of the interaction Hamiltonian is

$$|H_{fb}^{(\lambda)}|^2 = \frac{2\pi e^2}{kL^3} |J_\lambda^{fb}|^2 , \qquad (4b)$$

with $e^2 = \frac{1}{137}$ and

$$J_\lambda^{fb} = \int_{crystal} \psi_b^\dagger(\mathbf{r})(\alpha \cdot \hat{\epsilon}_\lambda)^* e^{-i\mathbf{k}\cdot\mathbf{r}} \psi_f(\mathbf{r}) d^3 r . \qquad (4c)$$

Here, $\hat{\epsilon}_\lambda$ is the photon polarization vector and $\alpha = (\alpha_1, \alpha_2, \alpha_3)$, each α_i being the usual Dirac matrix.

III. KINEMATICS

We will assume that the initial direction of the electron is almost parallel to the crystal (z) axis, so that $\theta \ll 1$, where θ is the angle between $\hat{p}$ and $\hat{z}$. In addition, we will assume that the photon is emitted in a direction close to forward $(k_z = k \cos\theta_k, \theta_k \ll 1)$, which is usually the case for $\gamma \equiv E/m \gg 1$, and that its energy lies in the lower part of the spectrum $(k \ll p)$, which is also the case for coherent bremsstrahlung and for the prominent peaks of channeling radiation.[8,12–14] One can then approximately separate the electron energy into longitudinal and transverse parts:

$$E \cong E_z + E_\perp , \qquad (5a)$$

where

$$E_z = (p_z^2 + m^2)^{1/2} , \qquad (5b)$$

and where the transverse energy $E_\perp(\mathbf{p}_\perp)$ is nonrelativistic, being given by

$$E_\perp(\mathbf{p}_\perp) = \frac{\mathbf{p}_\perp^2}{2\gamma m} \tag{5c}$$

for free electrons, while for bound electrons (e.g., bound by a single string), $E_\perp(\mathbf{p}_\perp)$ must be computed numerically. Under the further assumption that $k_\perp/k \ll 1/\gamma$ (satisfied if $\theta_k \ll 250$ mr for 2 MeV, $\ll 100$ mr for 5 MeV, $\ll 25$ mr for 20 MeV, or $\ll 10$ mr for 50 MeV electrons, respectively), one finds the photon energy (in the laboratory system) of the transition[8,13]

$$k = 2\gamma^2(E_\perp - E_\perp') , \tag{6}$$

an equation first derived by Andersen *et al.*[13] which is valid for fb, bb, and ff transitions.

An alternative derivation of the fb transition energy can be given which is specifically tailored to such transitions. In this derivation, we use Eqs. (1a) and (4a) to infer the energy and momentum conservation equations

$$p_z = p_z' + k , \tag{7a}$$

$$E = E' + k . \tag{7b}$$

Solving Eq. (3a) for the final-electron energy and using the above-mentioned approximation yields

$$E' \cong E_z' + \epsilon' , \tag{8a}$$

so that

$$E_z + \frac{\mathbf{p}_\perp^2}{2E_z} \cong E_z' + \epsilon' + k . \tag{8b}$$

This leads to

$$k_{nl} \cong \frac{(\mathbf{p}_\perp^2/2E) + |\epsilon_{nl}|}{1 - \beta_z \hat{k}_z} , \tag{8c}$$

where $\beta_z = p_z/E_z$. This expression is essentially the

same, within our approximation, as Eq. (6), see below.

Knowing the bound or continuum-state energies of a lattice string, Eq. (6) provides the photon transition energies as functions of the angle of incidence θ, supposed sufficiently small in the following. The characteristic variation of these energies with θ clearly identifies a given transition peak as corresponding to an ff, fb, or bb transition. Indeed, bb transitions yield photon energies which are essentially angle independent, since here both values of $E_\perp$ in Eq. (6) are then essentially the constant (or narrow-band, for the case of Bloch functions) initial and final bound-state energies. On the other hand, fb transitions from initial states of sufficiently high transverse energy show a parabolic dependence on θ, since such initial energies are well approximated in the laboratory system by[13]

$$E_\perp(\mathbf{p}_\perp) \cong \frac{\mathbf{p}_\perp^2}{2\gamma m} + U_0 , \tag{9a}$$

$p_\perp \equiv |\mathbf{p}_\perp| = p\sin\theta \cong p\theta$, where U_0 is the average lattice potential caused by the overlap of neighboring string potentials, while $E_\perp'$ is the constant energy of the bound final state. Finally, ff transitions, i.e., coherent bremsstrahlung proper, yield photon energies depending approximately linearly on θ, since k is proportional to the difference of the initial and final transverse energies $E_\perp$ and $E_\perp'$, respectively, and each of these energies depends on θ in an approximately quadratic fashion, as in Eq. (9a).

Figure 1 presents an example of such a dependence of fb and bb transition photon energies on θ.[8,15] The figure corresponds to electrons of 3.5-MeV kinetic energy, incident roughly parallel to the $\langle 100 \rangle$ axis of Si, making an angle θ with this axis. Table I shows the experimental energies[13] of the five transversely bound states (in the laboratory system) that exist in this case; the corresponding
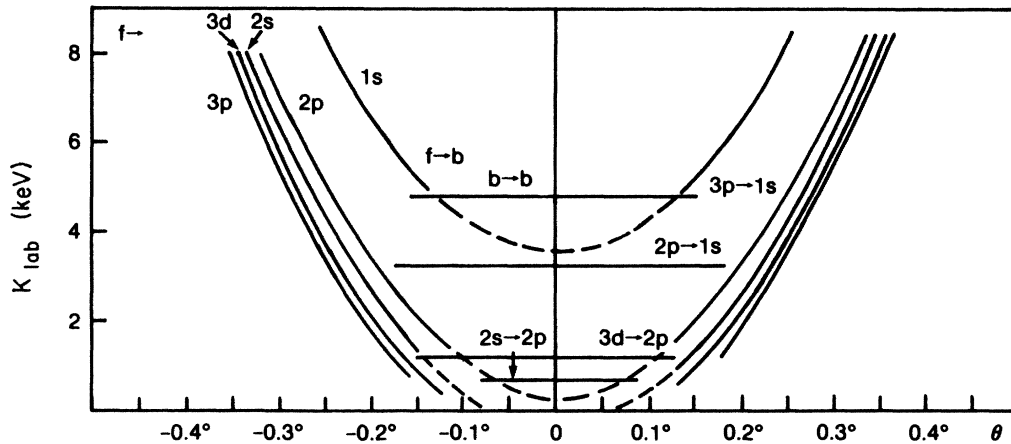
FIG. 1. Calculated laboratory photon energies as a function of the angle of incidence θ of various free-bound and bound-bound transitions as indicated, for the case of 3.5-MeV electrons incident close to the $\langle 100 \rangle$ axis in Si. For the fb transitions, an empirical average lattice potential $U_0 = -13.9$ eV (in the lab system) was used.

TABLE I. Experimental (column 1) and theoretical (columns 2 and 3) bound-state energies of transverse motion in the laboratory system for 3.5-MeV electrons incident close to the $\langle 100 \rangle$ axis of a Si crystal (superscript SS and MB indicate theoretical level energies obtained using single-string and multibeam potentials, respectively).

Bound state	ϵ_{nl}^{exp} (eV)	ϵ_{nl}^{SS} (eV)	ϵ_{nl}^{MB} (eV)
1s	−43.0	−42.81	−43.28
2p	−16.2	−13.77	−16.12
2s	−10.6	−7.07	−9.95
3d	−6.5		
3p	−4.1		

average potential in the lab system is $U_0 = -13.9$ MeV. The figure shows the calculated parabolic θ dependence of the energy k of the fb photon transition to the 1s, 2p, 2s, 3d, and 3p states, as well as the θ independent 3p-1s, 2p-1s, 3d-2p, and 2s-2p bb transition energies. From Eqs. (6) and (9a), the fb energy is given by

$$k = 2\gamma^2 \left[\frac{p^2\theta^2}{2\gamma m} + U_0 + |\epsilon| \right] ; \qquad (9b)$$

hence, k is parabolic in θ for $\theta \ll 1$, as is the case here. Equation (9) which follows from Eq. (6), agrees with Eq. (8c) as mentioned, if the empirical average lattice potential U_0 is introduced in Eq. (8c) also.

IV. CALCULATION OF TRANSITION PROBABILITIES

The transition probabilities can be calculated for fb and bb transitions in a unified way. Consider first bb transitions. In this case, J_λ^{fb} in Eq. (4c) is replaced by J_λ^{bb}, defined by the latter equation, but with the transversely bound initial and final states ψ_b, ψ_b' [approximated by Eq. (1b) and an analogous equation] replacing ψ_f and ψ_b, respectively, in Eq. (4c):

$$J_\lambda^{bb} = \left[\frac{E+m}{2EL}\right]^{1/2} \left[\frac{E'+m}{2E'L}\right]^{1/2} \int d^2r_\perp \int dz \left\{ \left[\begin{pmatrix} u' \\ \sigma \cdot p_0' u' \\ \overline{E'+m} \end{pmatrix} \varphi_{n'l'}(r_\perp) \right]^\dagger (\alpha \cdot \hat{\epsilon}_\lambda^*) e^{-ik\cdot r} \begin{pmatrix} u \\ \sigma \cdot p_0 u \\ \overline{E+m} \end{pmatrix} \varphi_{nl}(r_\perp) e^{ip_z z} \right\} , \qquad (10)$$

where p_0' is as before. Hence,

$$J_\lambda^{bb} = \frac{2\pi}{L} \left[\frac{E+m}{2E}\right]^{1/2} \left[\frac{E'+m}{2E'}\right]^{1/2} \delta(p_z - p_z' - k_z) \int d^2r_\perp e^{-ik_\perp\cdot r_\perp} (u')^\dagger \left[\varphi_{n'l'}^*, \frac{\sigma \cdot (p_0'\varphi_{n'l'})^\dagger}{E'+m} \right] (\alpha \cdot \hat{\epsilon}_\lambda^*) \begin{pmatrix} u \\ \sigma \cdot p_0 u \\ \overline{E+m} \end{pmatrix} \varphi_{nl} .$$

$$(11)$$

By comparing the wave functions ψ_f and ψ_b of Eqs. (1a) and (1b), it is seen that the fb transition matrix element J_λ^{fb} of Eq. (4c) can be obtained from the bb matrix element J^{bb} of Eq. (11) by the substitutions

$$p_0 \rightarrow p , \qquad (12a)$$

$$\varphi_{nl}(r_\perp) \rightarrow \frac{1}{L} e^{ip_\perp \cdot r_\perp} . \qquad (12b)$$

This will permit us to obtain the fb matrix element from the calculated bb matrix element.
Continuing with the calculation of the latter, Eq. (11), we find by using

$$\alpha = \begin{pmatrix} 0 & \sigma \\ \sigma & 0 \end{pmatrix} \qquad (13a)$$

that

$$J_\lambda^{bb} = \frac{2\pi}{L} \left[\frac{E+m}{2E}\right]^{1/2} \left[\frac{E'+m}{2E'}\right]^{1/2} \delta(p_z - p_z' - k_z)$$

$$\times \int d^2r_\perp e^{-ik_\perp\cdot r_\perp} (u')^\dagger \left[\varphi_{n'l'}^*(r_\perp) \frac{\hat{\epsilon}_\lambda^* \cdot p_0 + i\sigma \cdot (\hat{\epsilon}_\lambda^* \times p_0)}{E+m} \varphi_{nl}(r_\perp) + \frac{(p_0'\varphi_{n'l'})^\dagger \cdot \hat{\epsilon}_\lambda^* + i\sigma \cdot [(p_0'\varphi_{n'l'})^\dagger \times \hat{\epsilon}_\lambda^*]}{E'+m} \varphi_{nl}(r_\perp) \right] u .$$

$$(13b)$$

We now define the matrix elements

$$\hat{I}_{n'l',nl}(k_\perp) = \int d^2r_\perp e^{-ik_\perp\cdot r_\perp} \varphi_{n'l'}^*(r_\perp) p_0 \varphi_{nl}(r_\perp) , \qquad (14a)$$

$$\hat{I}'_{n'l',nl}(k_\perp) = \int d^2r_\perp e^{-ik_\perp\cdot r_\perp} \varphi_{n'l'}^*(r_\perp) (p_0 - k) \varphi_{nl}(r_\perp) , \qquad (14b)$$

and

$$I_{nl}(q_\perp) = \int d^2r_\perp e^{iq_\perp\cdot r_\perp} \varphi_{nl}^*(r_\perp) , \qquad (14c)$$

where

$$q = p - k . \qquad (14d)$$

The substitutions of Eqs. (12), which transform J_λ^{bb} into J_λ^{fb}, then entail

$$\mathbf{I}_{n'l',nl}(\mathbf{k}_\perp) \rightarrow (p/L)I_{nl}(\mathbf{q}_\perp) , \tag{15a}$$

$$\mathbf{I}'_{n'l',nl}(\mathbf{k}_\perp) \rightarrow (q/L)I_{nl}(\mathbf{q}_\perp) . \tag{15b}$$

It is now straightforward to evaluate the integral $\int_1$ in Eq. (13b) which corresponds to the term with denominator $E + m$; it is

$$\int_1 = \frac{1}{E+m}\{[(u')^\dagger u]\hat{\epsilon}_\lambda^* \cdot \hat{\mathbf{I}}_{n'l',nl}$$
$$+ i[(u')^\dagger \sigma u]\cdot(\hat{\epsilon}_\lambda^* \times \hat{\mathbf{I}}_{n'l',nl})\} . \tag{16a}$$

For evaluating the second integral $\int_2$ with denominator $E' + m$, we use partial integration, which leads to

$$\int_2 = \frac{1}{E'+m}\{[(u')^\dagger u]\hat{\epsilon}_\lambda^* \cdot \mathbf{I}'_{n'l',nl}$$
$$+ i[(u')^\dagger \sigma u]\cdot(\mathbf{I}'_{n'l',nl} \times \hat{\epsilon}_\lambda^*)\} . \tag{16b}$$

Accordingly,

$$J_\lambda^{bb} = \frac{2\pi}{L}\left[\frac{E+m}{2E}\right]^{1/2}\left[\frac{E'+m}{2E'}\right]^{1/2}\delta(p_z - p'_z - k_z)$$

$$\times (u')^\dagger\left[\frac{\hat{\epsilon}_\lambda^* \cdot \mathbf{I}_{n'l',nl} + i\sigma\cdot(\hat{\epsilon}_\lambda^* \times \mathbf{I}_{n'l',nl})}{E+m} + \frac{\hat{\epsilon}_\lambda^* \cdot \mathbf{I}'_{n'l',nl} - i\sigma\cdot(\hat{\epsilon}_\lambda^* \times \mathbf{I}'_{n'l',nl})}{E'+m}\right]u . \tag{17a}$$

Next we average $|J_\lambda^{bb}|^2$ over initial electron polarizations and sum it over final electron and photon polarizations, since at this point we are not interested in studying polarization effects. The result is found to be

$$\sum \langle |J_\lambda^{bb}|^2 \rangle = \frac{4\pi}{L}\frac{E+m}{2E}\frac{E'+m}{2E'}\delta(p_z - p'_z - k_z)\left[\frac{|\mathbf{I}_{n'l',nl}|^2}{(E+m)^2} + \frac{|\mathbf{I}'_{n'l',nl}|^2}{(E'+m)^2} - \frac{2\text{Re}\hat{k}\cdot\mathbf{I}^*_{n'l',nl}\hat{k}\cdot\mathbf{I}'_{n'l',nl}}{(E+m)(E'+m)}\right] . \tag{17b}$$

We now proceed to evaluate the cross section of the transitions. This is obtained from dI_λ, Eq. (4a), by dropping the factor k, and dividing by the incident electron current, which is β_z/L^3. Expressing the energy-conservation δ function in a well-known way in terms of one containing $\delta(k - k_{nl})$, with k_{nl} given by Eq. (8c) and carrying out the appropriate integrations, one has

$$\frac{1}{L}\frac{d\sigma_{bb}}{d\Omega_k} = \frac{e^2}{4\pi}L^2\frac{k}{pE'}\frac{1}{1-(q_z/E'_z)\hat{k}_z}\left[\frac{E'+m}{E+m}|\mathbf{I}_{n'l',nl}|^2 + \frac{E+m}{E'+m}|\mathbf{I}_{n'l',nl}|^2 - 2\text{Re}\hat{k}\cdot\mathbf{I}^*_{n'l',nl}\hat{k}\cdot\mathbf{I}'_{n'l',nl}\right] . \tag{18a}$$

From this, and making the substitutions in Eqs. (15), one can now obtain the free-bound cross section:

$$\frac{1}{L}\frac{d\sigma_{fb}}{d\Omega_k} = \frac{e^2}{4\pi}\frac{k}{pE'}\frac{|I_{nl}(\mathbf{q}_\perp)|^2}{1-(q_z/E'_z)\hat{k}_z}\left[\frac{E'+m}{E+m}p^2 + \frac{E+m}{E'+m}q^2 - 2\hat{k}\cdot\mathbf{p}\hat{k}\cdot\mathbf{q}\right] . \tag{18b}$$

In view of the presence of the factor $1/L$ on the left-hand side of Eq. (18b) and of the fact that the corresponding right-hand side is independent of L, the quantity $(1/L)(d\sigma_{fb}/d\Omega_k)$ can be interpreted as the cross sections per string of length L. However, $(1/L)(d\sigma_{bb}/d\Omega_k)$ in Eq. (18a) cannot be interpreted in this way, since the corresponding right-hand side is proportional to L^2. The source of this difficulty is that here the initial state is transversely bound, while cross sections are usually defined with respect to an incident plane wave. Physically, there is such a plane electron wave externally incident on the crystal; when penetrating the latter, it will populate the various transversely bound levels in a well-defined fashion, and the excited bound states will then undergo transitions to lower levels, as described by Eq. (18a). In order to obtain the experimentally measurable cross section for bb transitions due to incident electrons, one has to multiply each $d\sigma_{bb}$ by the corresponding initial-state population. This will be done in the following.

The incident wave function is the same plane wave ψ_f for both fb and bb transitions; in the latter case, however, it first populates bound states $\psi_b(n,l)$ which in turn transit radiatively to appropriate lower-level bound states. The population of the former bound states is given by

$$\Pi_{nl} = |A_{nl}|^2 , \tag{19a}$$

where

$$A_{nl} = \int \psi_b^\dagger(n,l)\psi_f \, d^3r . \tag{19b}$$

By Eqs. (1a), (14c), (19a), and (19b), we find

$$\Pi_{nl} = \frac{1}{L^2}|I_{nl}(\mathbf{p}_\perp)|^2 . \tag{19c}$$

Accordingly, the experimentally relevant cross section for the bb transitions induced by the incident plane wave of Eq. (1) is

$$\frac{1}{L}\Pi_{nl}\frac{d\sigma_{\mathrm{bb}}}{d\Omega_k}=\frac{e^2}{4\pi}\frac{k}{pE'}\frac{1}{1-(q_z/E_z')\hat{k}_z}\,|\,I_{nl}(\mathbf{p}_\perp)\,|^2$$

$$\times\left[\frac{E'+m}{E+m}\,|\,\mathbf{I}_{n'l',nl}(\mathbf{k}_\perp)\,|^2+\frac{E+m}{E'+m}\,|\,I'_{n'l',nl}(\mathbf{k}_\perp)\,|\,-2\mathrm{Re}\hat{k}\cdot\hat{\mathbf{I}}_{n'l',nl}(\mathbf{k}_\perp)\hat{k}\cdot\mathbf{I}'_{n'l',nl}(\mathbf{k}_\perp)\right]\,,\tag{19d}$$

from which the factor L^2 has disappeared. This equation is on a par with the fb cross section given by Eq. (18).

V. NUMERICAL EVALUATION AND COMPARISON WITH EXPERIMENT

Experiments demonstrating the presence of free-bound transitions in axial channeling radiation were carried out by the Aarhus group (see the second of Ref. 13). Their results are shown in Fig. 2, reproduced from that reference. They are presented as a graph of the laboratory photon spectra, plotted both versus photon energy k and angle of incidence θ of a 3.5-MeV electron beam with the $\langle 100\rangle$ direction in a 0.3-μm (top of the figure) and a 2-μm (bottom) Si crystal.

The experimental maxima or "mountain ridges" in this graph are seen to follow the kinematical relations shown in Fig. 1. The high ridges that also contain a pair of peaks symmetric about $\theta=0$ correspond to bb transitions, and lie above the constant-k lines of Fig. 1, while lower, horseshoe-shaped ridges opening up away from the bb ridges represent the fb transitions, which lie above the parabolas of Fig. 1. Actually, only the $f\to 1s$ transition is clearly visible, but some indications of the $f\to 2p$ and other higher fb transitions are present, especially in the upper part of Fig. 2.

In Fig. 3 we compare the theoretical and experimental fb kinematics. The experimental Aarhus ridges are shown as a shaded band for the $3p\to 1s$ transition and as a dashed line parabola for the $f\to 1s$ transition. For $U_0=0$, the solid theoretical $f\to 1s$ curve would have its vertex rest on the short horizontal dashed line at $k=5.30$

FIG. 2. Photon spectra in the laboratory, plotted both vs photon energy k and angle of incidence θ, as observed experimentally by the Aarhus group, second reference of Ref. 13. They were obtained with 3.5-MeV electrons incident at an angle θ with a $\langle 100\rangle$ axis in a 0.3-μm (top) and a 2-μm (bottom) Si crystal.
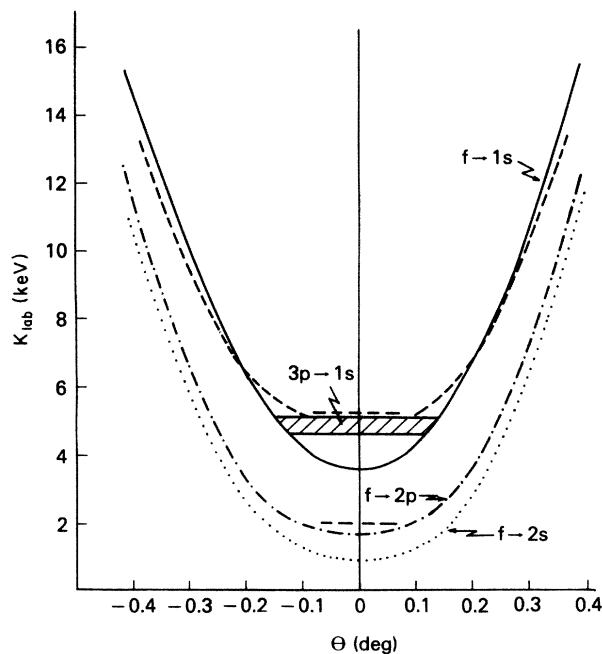
FIG. 3. Angular dependence of the photon energy in the laboratory for 3.5-Me electrons incident at an angle θ with the $\langle 100\rangle$ axis in a Si crystal. Dashed line: experiment and multibeam calculation, $f\to 1s$ transition. Solid line: parabolic approximation Eq. (9a) for $f\to 1s$ transition. Dash-dotted line: approximation for $f\to 2p$ transitions obtained by shifting dashed curve inside crossover points and solid curve outside crossover points by $2\gamma^2(\epsilon_{2p}^M-\epsilon_{1s}^M)=3.35$ keV. Dotted line: Approximation for $f\to 2s$ transition obtained by shifting dashed curve inside crossover points and solid curve outside crossover points by $2\gamma^2(\epsilon_{2s}^M-\epsilon_{1s}^M)=4.11$ keV. Shaded band: Experimental $3p\to 1s$ bb-transition line.

keV which represents the continuum boundary. The theoretical wings of the parabola would then lie considerably above the experimental values. Introduction of the prevailing average lattice potential $U_0 = -13.9$ eV removes this discrepancy in the wings, requiring however some flattening out around $\theta = 0$. Without such a flattening out, the $f \rightarrow 2s$ and higher fb transition energies would dip below $k = 0$ at the centers of their parabolas (see Fig. 1). In fact, the angle dependence of the photon energy obtained from a many-beam calculation (see Fig. 10, second of Ref. 13) shows that the photon energy for $\theta = 0$ is underestimated by Eq. (9a) by 1.31 keV. The inadequacy of Eq. (9a) near $\theta = 0$ is not surprising since it was derived under the assumption that the transverse kinetic energy of the electron is large enough so that the crystal potential may be treated as a perturbation. For $E = 4.011$ MeV and $U_0 = -13.9$ eV the condition $T \gg |U_0|$ requires $|\theta| \gg 0.15°$. From Eq. (3) it is seen that the solid parabola given by Eq. (9a) and the dashed experimental curve (which closely coincides with the result of a multibeam calculation which was carried out in the second of Ref. 13) intersect at $\theta \approx 0.25°$. Thus by using the dashed curve for $|\theta| < 0.25°$ and Eq. (9a) for $|\theta| \geq 0.25°$ one obtains realistic values of k for small angles, and one has a good approximation for large angles and a smooth transition between the two regions. The angular dependence of k thus defined was used in our calculation of the $f \rightarrow 1s$ spectra. For the $f \rightarrow 2p$ and $f \rightarrow 2s$ transitions, photon energies used were as indicated in Fig.

3. These curves were obtained by shifting the $f \rightarrow 1s$ angular dependence down by $2\gamma^2(\epsilon_{2p} - \epsilon_{1s})$ and $2\gamma^2(\epsilon_{2s} - \epsilon_{1s})$, respectively, these level differences being given by the multibeam calculation (see below).

For our calculation of the fb strength Eq. (18b) was used, assuming $\mathbf{k} \| \mathbf{p}$ throughout. Although we used the exact Eq. (18b), it is instructive to note its approximate form for $\mathbf{k} \| \mathbf{p}$, $\theta \ll 1$, and $k \ll E$ as it was the case for the Aarhus experiment, since then a clearer view of the dependence of the cross section on its various variables emerges. One finds in this approximation:

$$\frac{1}{L} \frac{d\sigma_{fb}}{d\Omega_k}\bigg|_{\mathbf{k}\|\mathbf{p}} \cong \frac{e^2}{4\pi p} \frac{E}{E+m-k} \frac{2k^3}{E-k} \frac{|I_{nl}(\mathbf{q}_\perp)|^2}{1+(2k/p)+\theta^2} ,$$

(20a)

or, still to good accuracy (a few percent for the larger values of θ in the figures):

$$\frac{1}{L} \frac{d\sigma_{fb}}{d\Omega_k}\bigg|_{\mathbf{k}\|\mathbf{p}} \cong \frac{e^2}{4\pi p} \frac{2k^3}{E+m} |I_{nl}(\mathbf{q}_\perp)|^2 .$$

(20b)

Using Eqs. (2a) and (14c), we obtain:

$$I_{nl}(\mathbf{q}_\perp) \equiv I_{nl}(q_\perp)$$

$$= (2\pi)^{1/2} e^{-il(\Phi - \pi/4)}$$

$$\times \int_0^\infty J_l(q_\perp \rho) R_{nl}^*(\rho) \rho \, d\rho ,$$

(21)
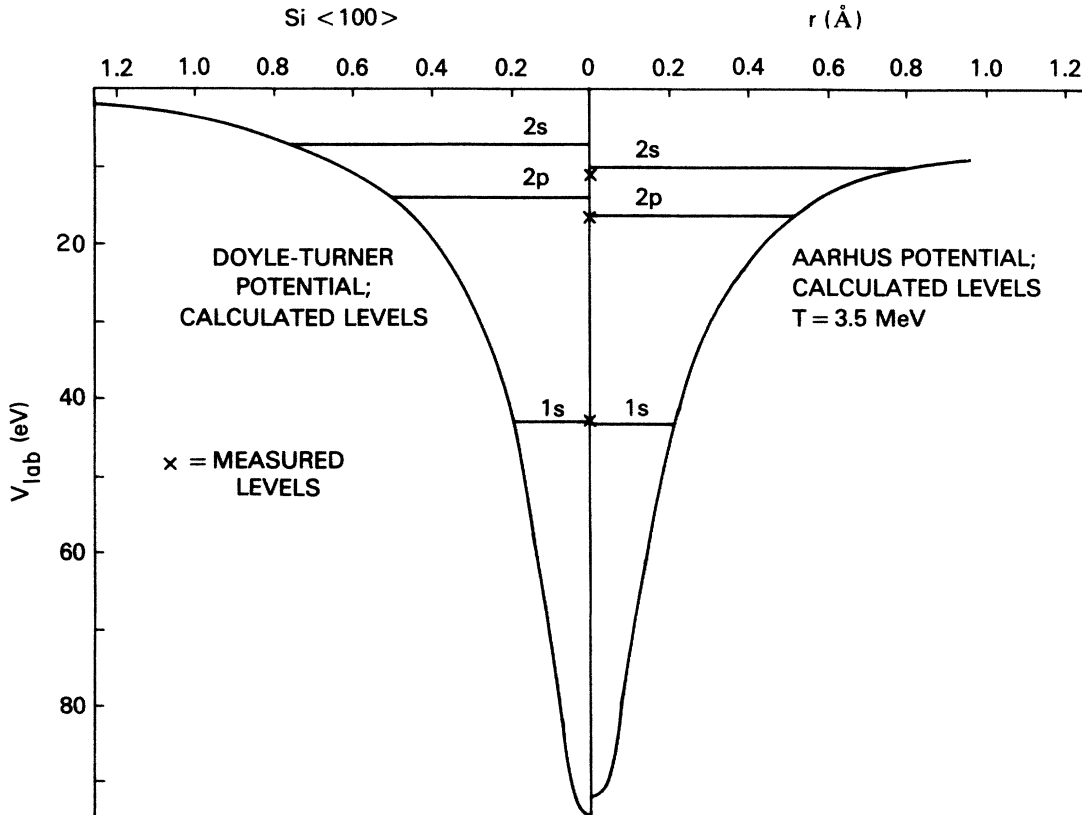
FIG. 4. Doyle-Turner string potential and corresponding calculated levels (left-hand side); Aarhus potential and resulting calculated levels (right-hand side) for 3.5-MeV electrons incident close to the $\langle 100 \rangle$ axis in a Si crystal.

where the inconsequential phase Φ is the polar angle of $q_\perp$ in the $r_\perp$ plane.

We evaluated the radial wave function $R_{nl}(\rho)$ numerically by solving the radial Schrödinger equation corresponding to Eq. (2b) with suitable string potentials $V(\,|\,r_\perp\,|\,) \equiv V(\rho)$. An appropriate single-string potential for Si is given by Eq. (21) of the second reference of Ref. 13, with the parameters listed in Table I of that reference (we adopted the first set of their parameters a_i, b_i, and $\rho = 0.1$ Å). This is the Doyle-Turner potential, shown on the left-hand side of Fig. 4 together with the energy levels obtained from our solution of the transverse Schrödinger equation. These levels are also shown in the column labeled ϵ_{nl}^{ss} in Table I. The right-hand side of Fig. 4 shows the continuum potential due to the entire crystal in the direction towards the nearest-neighbor string (scaled to 3.5 MeV from the second reference of Ref. 13). Solving the Schrödinger equation with this potential yields the energy levels shown on the right-hand side of Fig. 4 and in the column ϵ_{nl}^{MB} in Table I. It is seen that the lowest
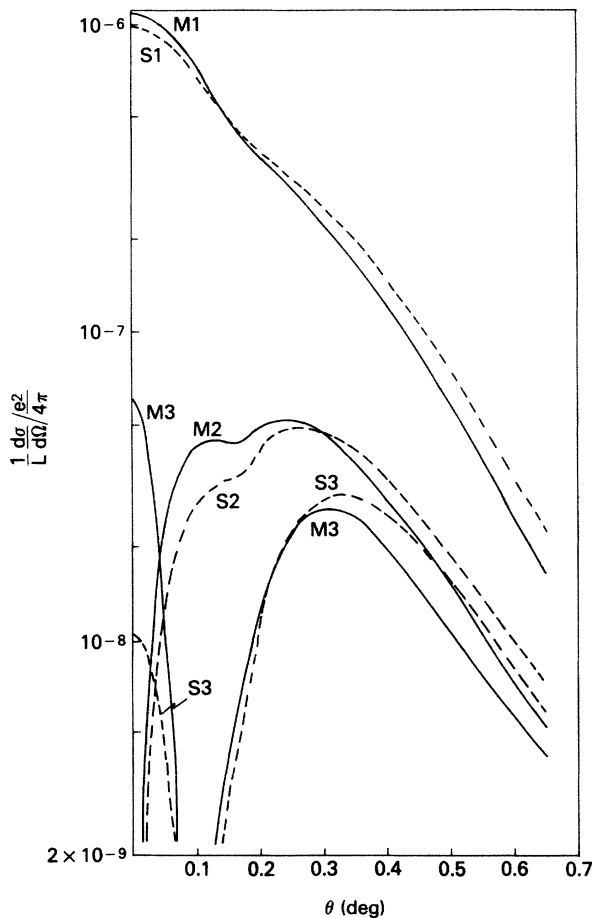
FIG. 5. Forward photon intensity for $f \to 1s$ (curves $M1$ and $S1$), $f \to 2p$ (curves $M2$ and $S2$), and $f \to 2s$ (curves $M3$ and $S3$) transitions of 3.5-MeV electrons incident at an angle θ with the $\langle 100 \rangle$ axis of a Si crystal. Solid curves ($M1$, $M2$, $M3$): results based on multibeam potential. Dashed curves ($S1$, $S2$, $S3$): results based on single-string potential.

($1s$) level predicted by both potentials is in close agreement with the experimental value, but that in general, as expected, the levels due to the multibeam potential deviate less from the experimental values ϵ_{nl}^{exp} than those corresponding to the single-string potential. ("Absolute" experimental values ϵ_{nl}^{exp} were obtained from the experimental transition energies of the second reference of Ref. 13 by normalizing with U_0).

With the wave functions thus obtained, we evaluated I_{nl} of Eq. (14), and subsequently the forward cross section $(d\sigma/d\Omega_k)_{0'}/L(e^2/4\pi)$ of Eq. (20b) for all three transitions investigated. The dashed lines (labeled $S1$, 2, 3) shown in Fig. 5 correspond to the results based on the single-string potential, the solid lines (labeled $M1$, 2, 3) to those using the multibeam potential, which we took from the second Ref. 13 in scaled numerical form, using it as an effective, realistic potential for our single-string calculation. In order to facilitate a better comparison of these results with those in Fig. 2, we depict the same result on a three-dimensional graph above the k-θ plane in Fig. 6, where the curves of $(d\sigma/d\Omega_k)_{0'}/L(e^2/4\pi)$ are plotted in the form of horseshoe-shaped ridges as in Fig. 2. The qualitative agreement of our calculation with the experiment is evident if one observes that the two extra peaklets on both sides of $\theta = 0$ in Fig. 2 actually do not belong to the $f \to 1s$ ridge, but rather to the $3p \to 1s$ bb transition which kinematically overlaps the $f \to 1s$ parabola near $\theta = 0$ (see Fig. 3). The $f \to 1s$ horseshoe ridge is rather smooth in this region; in contrast, the $f \to 2p$ ridge goes through a null at $\theta = 0$, and the $f \to 2s$ ridge through a null at $\theta \cong \pm 0.1°$.

By inspecting these results, it becomes evident that more experiments, carried out with better resolution, will be needed in order to allow a quantitative comparison with theory. On the theoretical side, we are now extending our approach to a calculation of the bb transition spectra given by Eq. (20b), in order to effect a comparison with the experimental bb ridges of Fig. 2 with the same single-string model used here for the fb transitions. In addition, a calculation of the polarization of fb and bb radiation is in progress.
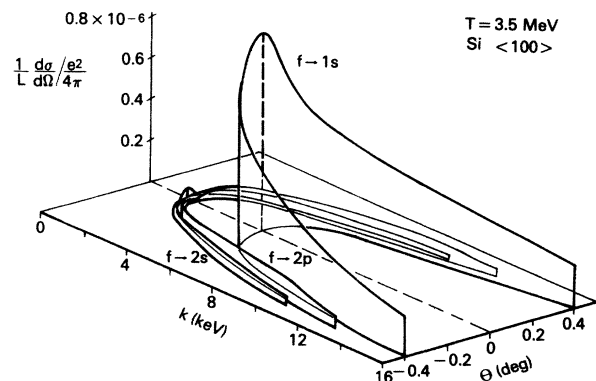
FIG. 6. Data of Fig. 5 plotted above the kinematic parabolas of Fig. 3, in order to facilitate comparison with the experimental results shown in Fig. 2.

VI. SUMMARY

Free-bound transitions in coherent bremsstrahlung-channeling radiation processes were observed experimentally,[13] but (with one exception for planar channeling) have hitherto not been analyzed theoretically. In this work, we have obtained analytic expressions for the spectral intensities of the photons emitted by axially channeled electrons, as well as for the analogous quantities in bound-bound transitions to which they may be compared. Numerical calculations have been carried out in order to obtain quantitative results for the photon intensities of specific transitions; the results are in good qualitative agreement with the available experiments.

[1]See, e.g., *Coherent Radiation Sources*, Vol. 38 of *Topics in Current Physics*, edited by A. W. Sáenz and H. Überall (Springer-Verlag, Berlin, 1985).

[2]See, e.g., W. Heitler, *The Quantum Theory of Radiation*, 3rd ed. (Clarendon, Oxford, 1954).

[3]E. J. Williams, Phys. Rev. **45**, 720 (1934).

[4]H. Überall, Phys. Rev. **103**, 1055 (1956).

[5]See also A. W. Sáenz and H. Überall, Phys. Rev. B **25**, 4418 (1982).

[6]G. Diambrini Palazzi, Rev. Mod. Phys. **40**, 611 (1968).

[7]H. Überall, Z. Naturforsch. **17A**, 332 (1962).

[8]See, e.g., A. W. Sáenz and H. Überall, *Theory of Coherent Bremsstrahlung*, Ref. 1.

[9]See, e.g., G. D. Kovalenko, L. Ya. Kolesnikov, and A. L. Rubashkin, *Coherent Bremsstrahlung-Experiment*, Ref. 1.

[10]J. Lindhard, K. Dan. Vidensk. Selsk. Mat. Fys. Medd. **34**, No. 14 (1965).

[11]M. A. Kumakhov, Phys. Lett. **57**, 17 (1976).

[12]R. L. Walker, B. L. Berman, and S. D. Bloom, Phys. Rev. A **11**, 736 (1975); M. J. Alguard, R. L. Swent, R. H. Pantell, B. L. Berman, S. D. Bloom, and S. Datz, Phys. Rev. Lett. **42**, 1148 (1979); see also B. L. Berman and S. Datz, *Channeling Radiation Experiments*, Ref. 1.

[13]J. U. Andersen, K. R. Eriksen, and E. Laegsgaard, Phys. Scr. **24**, 588 (1981); J. U. Andersen, E. Bonderup, E. Laegsgaard, B. B. Marsh, and A. H. Sørensen, Nucl. Instrum. Methods **194**, 209 (1982); see also J. U. Andersen, E. Bonderup, and E. Laegsgaard, *Channeling Radiation-Quantum Theory*, Ref. 1.

[14]G. Bologna, G. Diambrini Palazzi, and G. P. Murtas, Phys. Rev. Lett. **4**, 572 (1960); G. Barbiellini, G. Bologna, G. Diambrini Palazzi, and G. P. Murtas, *ibid.* **8**, 454 (1962).

[15]A. W. Sáenz, A. Nagl, and H. Überall, Nucl. Instrum. Methods B **13**, 23 (1986); A. W. Säenz, A. Nagl, and H. Überall, in *Relativistic Channeling*, edited by R. A. Carrigan and J. A. Ellison (Plenum, New York, 1987). Note that Fig. 10 in that latter paper is superseded by Fig. 6 of the present paper.